Available online at www.sciencedirect.com
ScienceDirect
Journal of Magnetic Resonance 185 (2007) 50–58
JMR Journal of Magnetic Resonance
www.elsevier.com/locate/jmr

Adiabatic ^{1}H decoupling scheme for very accurate intensity measurements in ^{13}C NMR

Eve Tenailleau, Serge Akoka *

LAIEM—CNRS UMR 6006, Faculté des Sciences et Techniques—Université de NANTES, 2 rue de la Houssinière—BP 92208, 44322 NANTES cedex 3, France

Received 8 August 2006; revised 10 November 2006
Available online 4 December 2006

Abstract

Adiabatic proton decoupling has been optimized in order to obtain accurate quantitative measurements of intensities on ^{13}C NMR spectra. For each offset, the minimum adiabaticity factor (Km) reached during the pulse was computed. This K_m profile was used to optimize the peak value and the swept frequency range of the adiabatic pulses. With a cosinus amplitude modulation, offset-independent-adiabaticity, and the M4P5–M4P9–M4P5′–M4P9′ phase cycle, an accuracy of 2‰ for the ^{13}C NMR measurements was reached. An approach using bi-labeled ^{13}C acetic acid and ethanol at 99% allowed a fine experimental determination of the uniformity of the decoupling profile. The comparison with WALTZ-16 highlights the improvements in the uniformity of the proton decoupling.

Keywords: ^{13}C NMR; Accuracy; Proton decoupling; Adiabatic pulses

1. Introduction

Quantitative ^{13}C NMR can be used for numerous applications like titrations, measurements of kinetic isotopic effects (KIE) [1], and authentication [2]. The acquisition conditions needed to obtain quantitative measurements with a precision of 1% are well known [3,4]. However, for applications such as quantification of ^{13}C isotopomers (i.e., isotopic distribution measurements for the elucidation of biosynthesis mechanisms at natural abundance), the order of the accuracy and precision required is about 1‰. Indeed, in natural conditions, the $^{13}C/^{12}C$ isotope ratios present a very restricted range of isotopic deviations: the difference in this ratio between two molecules, or two sites of the same molecule, is never higher than 50‰ and often close to a few per thousand. Moreover, to recognize such a small amount of ^{13}C nuclei, a signal-to-noise ratio greater than 1000 and a homogeneous response over all the effective bandwidth are essential.

It has been shown in previous works that inhomogeneous proton decoupling over the ^{1}H bandwidth constitutes a severe limitation for high accuracy in ^{13}C NMR [5]. Only adiabatic pulses present sufficient efficiency to reach this goal. Up to now, many developments have been proposed in order to perform an efficient adiabatic decoupling [6–11]. However, the aim of these works was to obtain a decoupling on wider and wider bandwidths with an accuracy of several percent. It was not the accurate quantification of ^{13}C intensities.

In the present work, we show that it is possible to define a proton decoupling scheme to reduce to a minimum the spectrum distortions introduced by imperfect broadband decoupling using adiabatic pulses. The optimization of the shape, the duration and the phase cycle is described to reach a very uniform ^{1}H decoupling. To assess the accuracy reached on the ^{13}C NMR intensity measurements, we used bi-labeled ^{13}C–^{13}C two-carbon molecules.

* Corresponding author. Fax: +33 251125712.
E-mail address: serge.akoka@univ-nantes.fr (S. Akoka).

1090-7807/$ - see front matter
doi:10.1016/j.jmr.2006.11.007

2. Method

2.1. Adiabatic pulses

During an adiabatic pulse with a duration T_p, the amplitude of the RF field is modulated between 0 and ω_2^{max} and the frequency is modulated from $-\Delta F$ to $+\Delta F$

$$\omega_2(\tau) = \omega_2^{max} f(\tau) \qquad \text{with} \quad \omega_2^{max} = \gamma B_2^{max}, \ \tau = \frac{t}{T_p} \text{ and } \tau \in \left[-\frac{1}{2}, \frac{1}{2}\right]$$

and $f(\tau)$ is a dimensionless function varying between 0 and 1.

$$\Delta\omega(\tau) = \Delta\omega^{max} g(\tau) \qquad \text{with} \quad \Delta\omega^{max} = 2\pi.\Delta F$$

and $g(\tau)$ is a dimensionless function varying between -1 and 1.

The adiabaticity factor at the reduced time (τ) and for the offset Ω, ($K(\Omega,\tau)$), is [11–13]:

$$K(\Omega,\tau) = \frac{\omega_{eff}(\Omega,\tau)}{\left|\frac{d\theta}{d\tau}\right|} \cdot T_p = \frac{T_p \cdot (\Delta\omega^{max})^2 \left[\left(\frac{\omega_2^{max} \cdot f(\tau)}{\Delta\omega^{max}}\right)^2 + \left(g(\tau) - \frac{\Omega}{\Delta\omega^{max}}\right)^2\right]^{\frac{3}{2}}}{\omega_2^{max}\left|\left(g(\tau) - \frac{\Omega}{\Delta\omega^{max}}\right)\left(\frac{df(\tau)}{d\tau}\right)_\tau - f(\tau)\left(\frac{dg(\tau)}{d\tau}\right)_\tau\right|} \tag{1}$$

It must be noted that $K(\Omega,\tau)$ is directly proportional to the pulse duration T_p. This is why (K/T_p) will be used below to discuss the influence of other parameters.

As can easily be seen from Eq. (1), the modulation functions $f(\tau)$ and $g(\tau)$ have a great impact on the evolution of K according to the reduced time τ or the offset Ω and many different combinations have been previously proposed [6,8,12–16]. In order to improve the efficiency of the adiabatic pulses at the extremities of the frequency bandwidth, some offset-independent-adiabaticity (OIA) pulses have been developed [11,12]. The $g(\tau)$ function is calculated from the $f(\tau)$ function according to:

$$g(\tau) = \frac{T_p \cdot \left(\omega_2^{max}\right)^2}{K^0 \Delta\omega^{max}} \int (f(\tau))^2 \, d\tau \tag{2}$$

where K^0 is the on-resonance adiabaticity (the adiabaticity obtained at τ_Ω when the pulse frequency is equal to the resonance frequency (i.e., $\Delta\omega^{max} g(\tau_\Omega) = \Omega$).

In such conditions, K^0 is independent of Ω and equal amounts of RF energy are delivered to every isochromat in the bandwidth [13]. In the following, this will be called the offset-independent-adiabaticity procedure (OIA).

2.2. Adiabatic decoupling

As we have already mentioned, the aim of this work is the optimization of the decoupling conditions in order to perform quantitative measurements of ^{13}C intensities with high accuracy (close to 1‰). The efficiency of an adiabatic decoupling scheme is driven by: (a) the ability of the adiabatic pulse to perform an inversion of the magnetization over the decoupled bandwidth, (b) the pulse duration, which must be short compared to the T_2 and the inverse of the coupling constant, (c) the pulse sequence preceding the decoupling sequence and finally (d) the phase cycle applied during decoupling to obtain compensation of the residual pulse imperfections [8,10,17]. An imperfect decoupling results in a residual splitting Jr; the aim of decoupling optimization is to reduce the value of Jr as much as possible in order to minimize its influence on the line shape.

Furthermore, some limitations have to be taken into account: (i) the maximum voltage permitted by the probe, which determines ω_2^{max} and (ii) the RF heating of the sample, which depends on the material inside the tube, the duty cycle of the decoupling and the energy deposed on the sample by one RF pulse determined by the root-mean-square value ω_2^{rms}.

The efficiency of an adiabatic pulse to rotate the magnetization from the $+z$ to the $-z$ position is closely related to the adiabaticity factor K. In agreement with previous work [13], Fig. 1 shows that K depends on τ and Ω. For each offset, the pertinent parameter seems, therefore, to be the minimum value K_m reached by K during the pulse [13]. It can be expected that, for a uniform efficiency, K_m needs to be independent of the value Ω inside the decoupling bandwidth.

For the purpose of this paper, we have examined four pulse shapes, the $f(\tau)$ and $g(\tau)$ functions of which are listed in Table 1. The evolution of $\frac{K(0,\tau)}{T_p}$ is plotted in Fig. 1a for these pulses. ω_2^{max} values were chosen in order to obtain the same ω_2^{rms} value for the four pulses and ΔF were chosen in order to obtain the same value of K^0 (Table 1). It can be observed that K_m is not always obtained on resonance as has been previously claimed in numerous papers [8,9,11,13,18]. Furthermore, Fig. 1b shows the evolution of $\frac{K(\Omega,\tau)}{T_p}$ for two offsets (center and extremity of the proton decoupled bandwidth at 500 MHz) for the cos/sin pulse. Here, K_m has different values and is not reached at the same time by the two isochromats.

In Fig. 2, the calculated values of K_m/T_p are plotted versus Ω for the four shapes studied. A calculation was made for Ω values covering the proton chemical shift at 500 MHz and the pulse parameters ω_2^{max} and ΔF were the same as for Fig. 1. The $g(\tau)$ functions were those given in Table 1 for Fig. 2a or those obtained from the offset-independent-adiabaticity (OIA) procedure (Eq. 2) for Fig. 2b. It appears that, in such conditions, the four pulses induce very different K_m profiles in terms of flatness and average value. However, in all cases, application of the OIA procedure significantly improves the flatness of the profile. Furthermore, a monotone and symmetric reduction of K_m is observed from the center (K_m^c) to the extremity (K_m^e) of the bandwidth. A flat K_m profile can

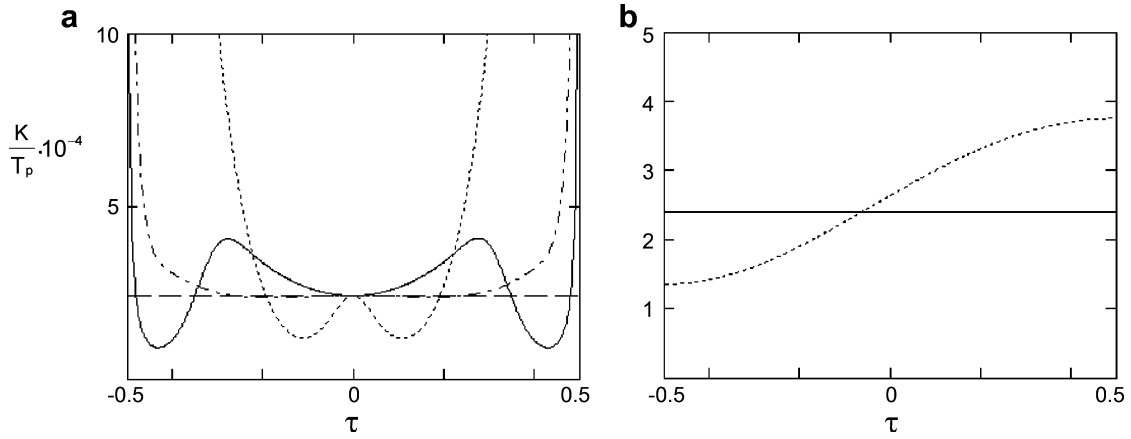

Fig. 1. Evolution of the reduced adiabaticity ($\frac{K}{T_p}$) during the pulse; (a) for different shapes and an isochromat at the center of the swept frequency range: Hyperbolic-secant (dotted line), tanh/tan (dotted and dashed line), WURST-20 (solid line) and cos/sin (dashed line). ω_2^{max} and ΔF are those indicated in Table 1 (same ω_2^{rms} and $\frac{K^0}{T_p} = 2.4\ 10^4\ s^{-1}$ for the four pulses). (b) for a cos/sin adiabatic pulse for two isochromats: at the center of the swept frequency range (solid line) and at the extremity of the swept frequency range (dashed line).

Table 1
Adiabatic full passage pulses

Shape	$f(\tau)$	$g(\tau)$	(ω_2^{max})[a] (kHz)	ΔF[b] (kHz)
HS	$f(\tau) = \mathrm{sech}(2.\beta.\tau)$[c]	$g(\tau) = \tanh(\beta.\tau)$	122.2	18.75
cos/sin	$f(\tau) = \cos(\pi \cdot \tau)$	$g(\tau) = \sin(\pi \cdot \tau)$	75.2	11.96
WURST-20	$f(u) = (1 - \lvert\sin(\pi\tau)\rvert^{20})$	$g(\tau) = 2 \cdot \tau$	60.0	12.14
tanh/tan	$f(\tau) = \tanh(\varepsilon\cdot(1 - \lvert 2\tau\rvert))$[d]	$g(\tau) = \frac{\tan(\kappa\cdot 2\tau)}{\tan(\kappa)}$[e]	56.0	137.00

[a] Calculated to obtain the same ω_2^{rms} for the four pulses.
[b] Calculated to obtain $K^0/T_p = 2.4 \times 10^4\ s^{-1}$.
[c] $\mathrm{sech}(\beta) = 0.01$.
[d] $\varepsilon = 10$.
[e] $\tan(\kappa) = 20$.

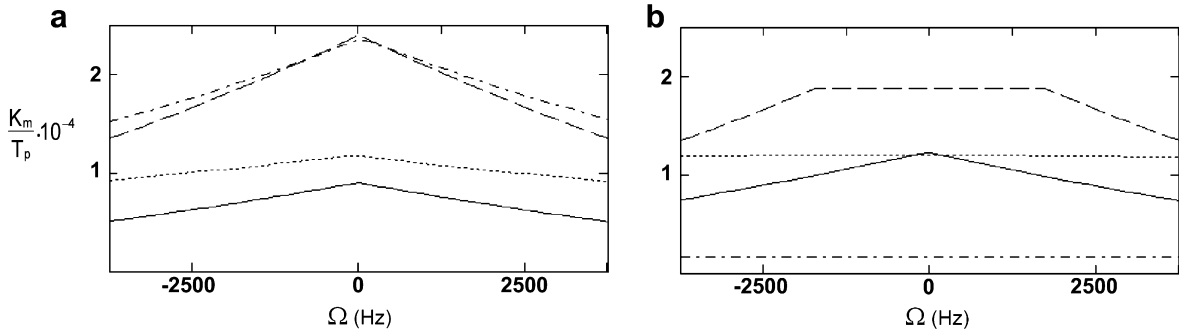

Fig. 2. Evolution of the minimum reduced adiabaticity ($\frac{K_m}{T_p}$) over the observed frequency range (corresponding to 12 ppm ^{1}H at 500 MHz). (a) for different shapes: hyperbolic-secant (dotted line), tanh/tan (dotted and dashed line), WURST-20 (solid line) and cos/sin (dashed line). (b) for adiabatic pulses with the same amplitude modulation functions as in (a) but with frequency modulation functions computed according to Eq. 2 in order to obtain an offset-independent-adiabaticity.

therefore be obtained if the following condition is fulfilled:

$$K_m^c - K_m^e \leqslant \xi \tag{3}$$

where ξ only depends on the accuracy desired.

Fig. 3 shows the evolutions of K_m^c/T_p and K_m^e/T_p with ΔF for the four shapes studied. As for Fig. 2, calculations were also made with $g(\tau)$ computed according to the OIA procedure. As can be observed in Fig. 3, for each shape there is a threshold value ΔF^{opt} above which Eq. 3 is fulfilled. The corresponding value of $\frac{K_m}{T_p}$ will be called $\frac{K_m^{opt}}{T_p}$ in the following and is therefore equivalent to the highest value of $\frac{K_m}{T_p}$ for which a flat K_m profile is obtained. Thus, the hypothesis of this work is that ΔF^{opt} is a good choice to obtain an efficient and uniform decoupling.

The values of ΔF^{opt} and $\frac{K_m^{opt}}{T_p}$ are indicated in Fig. 3 (dotted lines) and given in Table 2. The four shapes induce very different values of ΔF^{opt} and K_m^{opt}. However, when the OIA procedure is used, a significant reduction of the ΔF^{opt} dispersion is always observed. K_m^{opt} is quite different for the four pulses and the higher value is obtained for the cos/OIA shape.

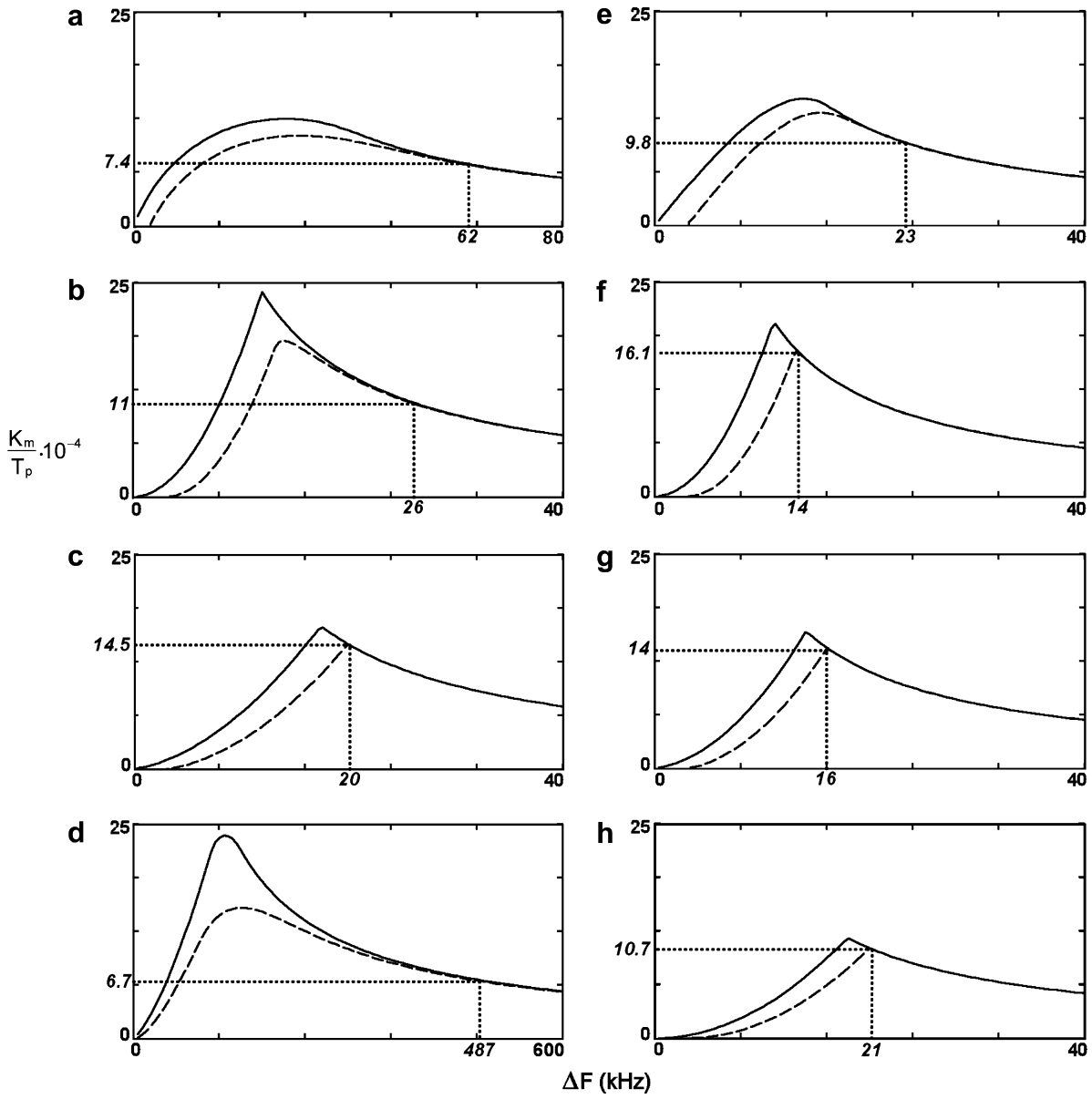

Fig. 3. Minimum reduced adiabaticity ($\frac{K_m}{T_p}$) as a function of the swept frequency range. $\frac{K_m}{T_p}$ was computed for two isochromats: at the center of the swept frequency range (solid line, $\frac{K^c_m}{T_p}$) and at the extremity of the swept frequency range (dashed line, $\frac{K^e_m}{T_p}$). Hyperbolic-secant (a), cos/sin (b), WURST-20 (c) and tanh/tan (d). Curves on the right (e–h) were computed with the same amplitude modulation functions as curves on the left but with frequency modulation functions computed according to Eq. (2) in order to obtain offset-independent adiabaticity. Dotted lines indicate ΔF^{opt} and $\frac{K^{opt}_m}{T_p}$ corresponding to the higher value of $\frac{K_m}{T_p}$ for which $\frac{K^c_m - K^e_m}{T_p} \leqslant 100\ s^{-1}$.

Table 2
Optimized parameters for flat K_m profiles

Shape	$\frac{K^{opt}_m}{T_p}$[a] ($10^4\ s^{-1}$)	ΔF_{opt}[a] (kHz)	Shape[b]	$\frac{K^{opt}_m}{T_p}$[a] ($10^4\ s^{-1}$)	ΔF_{opt}[a] (kHz)
HS	0.74	62	sech/OIA	0.98	23
cos/sin	1.1	26	cos/OIA	1.61	14
WURST-20	1.45	20	WURST/OIA	1.40	16
tanh/tan	0.67	487	tanh/OIA	1.07	21

[a] Corresponding to the higher value of $\frac{K_m}{T_p}$ for which $\frac{K^c_m - K^e_m}{T_p} \leqslant 100^{-1}\ s^{-1}$.
[b] With frequency modulation computed according to Eq. (2).

2.3. Comparison of experimental data

A sample of a bi-labeled ^{13}C–^{13}C two-carbon molecule contains four carbon isotopomers. Three are detectable by ^{13}C NMR and appear on the corresponding spectrum. On a proton decoupled ^{13}C NMR, the spectrum of the $^{13}C_1$–$^{13}C_2$ isotopomer presents two doublets and the spectrum of each mono-labeled isotopomer presents one

singlet. The isotopic enrichment only influences the ratios between the doublets and the singlets. However, the ratio (r) between the areas of the two doublets is an intra-molecular ratio and is therefore perfectly defined (1.000) [5].

We defined the parameter Δ as:

$$\Delta = (r - 1) \times 1000 \tag{4}$$

Accurate quantitative conditions for measurements of carbon site-specific isotopic ratios of bi-labeled two-carbon molecules are reached if $\Delta = 0‰$ is obtained over a full decoupler offset range. Thus, it appears that bi-labeled ^{13}C–^{13}C two-carbon molecules are good models to investigate the influence of acquisition conditions on the accuracy of the measurement, by studying the evolution of the parameter Δ with the distance between the decoupler offset and the proton resonance frequency.

As stated previously, the uniformity of the decoupling over the proton chemical shift range is a very important factor in the case of ^{13}C NMR quantitative measurements with high precision. In these conditions, the figures of merit previously proposed are not pertinent, so we use a new parameter L:

$$L = \frac{\sqrt{\sum_{i=1}^{n} \Delta_i^2}}{n} \tag{5}$$

with Δ, parameter defined above and n, number of explored frequencies.

The smaller the L parameter, the more the decoupling schemes enable Δ values close to zero to be obtained over all the observed frequency range. Thus, it corresponds to the decoupling conditions that allow accurate measurement of ^{13}C NMR intensities.

The demonstration of the efficiency of a decoupling strategy is usually performed by measuring the relative intensity of cycling sidebands versus the center band height [8,14,19–21]. This strategy is currently more accurate than measurement of the amplitude or the width of the center band [17]. Furthermore, these cycling sidebands can be undesirable in many applications because they can interfere with measured lines, especially when they come from very intense lines, such as those of solvent [19]. However, to measure ^{13}C intensities at natural abundance within a few per thousand, a signal-to-noise close to 1000 (or higher) is necessary. That requires very high concentrations and thus the solvent peaks have intensities of the same order as those of the analyzed molecules [2,5]. In addition, cycling sidebands are less intense at high power levels [19,20]. For these reasons, cycling sidebands are not detectable on ^{13}C NMR spectra performed on natural abundance and high concentration samples in the experimental conditions recommended in this paper (results not shown).

3. Results

First, bi-labeled acetic acid in D_2O solution was used. In this case, only one proton chemical shift is coupled to carbons. The ^{1}H–^{13}C coupling with the carbonyl carbon is very easy to remove because of its small J_{CH} coupling value. The parameter Δ is essentially driven by the efficiency of the methyl group decoupling. Furthermore, no ^{1}H–^{1}H homonuclear coupling is present thus avoiding interference by homonuclear Hartman–Hahn transfer [22].

We recorded on acetic acid ^{13}C NMR proton decoupled spectra using WURST-20 pulses with frequency modulation calculated according to Eq. (2) (OIA) and the M4P5 phase cycle: a nested combination of the MLEV phase cycle [23] and that proposed by Tycko et al. [24]. The ω_2^{max} values ranged from 24 to 56 kHz. The decoupling offset was chosen to equal the CH_3 proton frequency. For each spectrum, the Δ value was measured. The results are reported in Fig. 4a with the value of $1/K_m$ calculated for the same conditions. There is clearly a close correlation between $1/K_m$ and the uniformity of the decoupling. Then, the subsequent WURST-20 experiments were performed using a ω_2^{max} value of 56 kHz.

Next, the influence of the frequency range swept ΔF was studied. Proton decoupled ^{13}C NMR spectra were recorded for three ΔF ranges of 9, 20 and 29 kHz at 0, 1250 and 2500 Hz from the CH_3 proton frequency. For each spectrum, the Δ value was measured and compared to $1/K_m$. The results are plotted in Fig. 4b. Because the measured Δ values were found symmetrical on each side of the CH_3 proton offset, only positive offsets are shown. Like for the variation of ω_2^{max}, a close correlation can be observed between $1/K_m$ and the parameter Δ. Furthermore, the more accurate measurements on average of the three offsets correspond to $\Delta F = 20$ kHz, which is perfectly consistent with Fig. 3g. The same behavior of Δ versus ω_2^{max} and ΔF was observed for all the adiabatic shapes studied.

Next, the influence of the value of T_p was explored. Proton decoupled ^{13}C NMR spectra were recorded (ω_2^{max} value of 75.2 kHz and $\Delta F = 14$ kHz) at 0, 1250 and 2500 Hz from the CH_3 proton offset of the acetic acid. Several durations of the adiabatic sweep from 100 to 700 μs were tested. For these experiments, the phase cycle used was M4P5. The results are plotted in Fig. 5 for the adiabatic pulse cos/OIA. The more accurate measurements on three offsets were obtained for $T_p = 200$ μs with Δ values between 0‰ and 2‰. 100 and 300 μs gave acceptable Δ results between 0‰ and 4‰, whereas with 500 and 700 μs, the accuracy was about 6–10‰ in spite of the best values of on-resonance adiabaticity. The same results were obtained for the four studied pulse shapes.

To improve the efficiency of the decoupling, several phase cycles were tested. L was evaluated from 3 offsets (0, 1250 and 2500 Hz according to Eq. 5) for seven phase cycles. The results obtained for a 200 μs cos/OIA pulse are given in Table 3 with the number of phases for each cycle. The best decoupling efficiency was obtained with the phase cycle combination: M4P5–M4P9–M4P5′–M4P9′ [21]. When the same experiments were performed with $T_p = 600$ μs, the phase cycle M4P5 was found to be the more efficient.

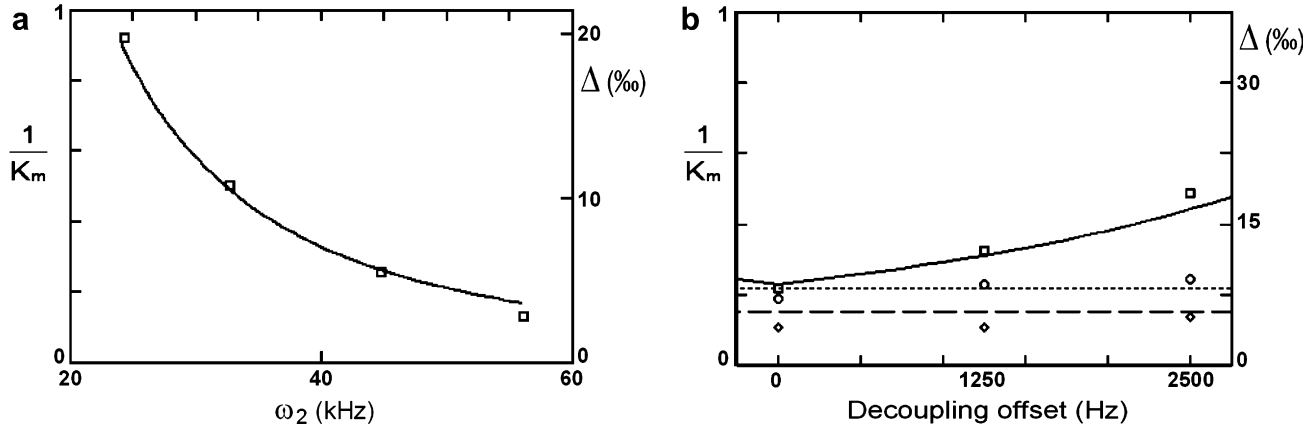

Fig. 4. Comparison between $1/K_m$ (lines) and Δ values in ‰ (□) obtained on the acetic acid molecule and for a WURST-20 pulse ($T_p = 700$ μs). (a) $\Delta F = 29$ kHz and ω_2^{max} ranged from 24 to 56 kHz. (b) $\omega_2^{max} = 56$ kHz and $\Delta F = 9$ (□), 20 (◇) and 29 kHz (○).

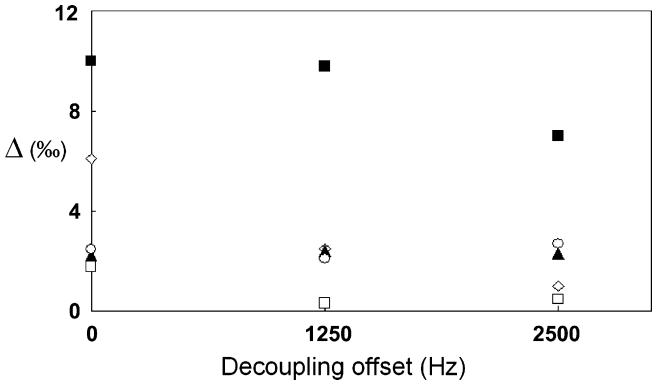

Fig. 5. Δ values (in ‰) for the acetic acid molecule and the decoupling sequence cos/OIA with $\omega_2^{max} = 75.2$ kHz, $\Delta F = 14$ kHz for three decoupling offsets, 0, 1250 and 2500 Hz, and five pulse durations: ◇ 100, □ 200, ▲ 300, ○ 500, ■ 700 μs.

Table 3
Efficiency of different phase cycles evaluated with the cos/OIA pulse ($\omega_2^{max} = 75.2$ kHz, $\Delta F = 14$ kHz, $T_p = 200$ μs)

Phase cycle	No. of phases in cycle	L
M_4P_5	20	1.06
M_4T_5	20	1.66
M_4P_9	36	2.43
$P_5P_5P_5$	125	0.75
P5P9	45	1.69
$M_4P_{5'}$	20	1.88
M_4P_5–M_4P_9–$M_4P_{5'}$–$M_4P_{9'}$	112	0.65

L was evaluated from three offsets (0, 1250 and 2500 Hz) according to Eq. (5).

Note: M4 = 0°, 0°, 180°, 180°; P5 = 0°, 150°, 60°, 150°, 0°; T5 = 0°, 120°, 60°, 120°, 0°; P9 = 0°, 15°, 180°, 165°, 270°, 165°, 180°, 15°, 0°; P5′ = 0°, 330°, 60°, 330°, 0°; P9′ = 0°, 195°, 180°, 345°, 270°, 345°, 180°, 195°, 0°.

Finally, the robustness of the optimized decoupling (cos/OIA, $\omega_2^{max} = 75.2$ kHz, $T_p = 200$ μs, $\Delta F = 14$ kHz, M4P5–M4P9–M4P5′–M4P9′) in relation to the presence of homonuclear coupling was evaluated by a comparison between the results obtained on bi-labeled acetic acid with those obtained on bi-labeled ethanol. Proton decoupled ^{13}C NMR spectra were recorded from −2.5 kHz to +2.5 kHz around the CH_3 proton offset for acetic acid and around the mean proton offset $(\nu_{CH_3} + \nu_{CH_2}/2)$ for ethanol. The same measurements were performed with WALTZ-16 for comparison. For each spectrum, the Δ value and L parameters were calculated. The results of Δ measurements are presented in Fig. 6. The cos/OIA decoupling gave very close results for the two molecules with Δ values lower than 2‰ inducing an L parameter of 0.42 and 0.44 for acid acetic and ethanol, respectively, while L values obtained with WALTZ-16 were 1.9 and 10.7.

4. Discussion

The results shown in Fig. 4 clearly demonstrate that K_m, the minimum adiabaticity for a given isochromat, is a good criterion to predict the best values of ω_2^{max} and ΔF for an efficient decoupling. The profile of $1/K_m$ over the decoupled frequency range is highly correlated to the uniformity of the proton decoupling. The optimal choice for these parameters can therefore be performed by simple computation, avoiding tedious experimental procedures.

Fig. 3 shows that the OIA procedure significantly increases the optimal value of K_m. The only exception is the WURST-20 pulse. However, in this case, the impact of the OIA procedure is very low. Furthermore, among the pulse shapes explored, the best results were obtained for the cos/OIA shape.

Conversely, K_m does not allow the determination of the best value for the pulse duration T_p as shown in Fig. 5. Because the adiabaticity K is directly proportional to T_p (Eq. 1), it could be expected that the decoupling efficiency would increase (or Δ decrease) when T_p is increased. This is not the case and Fig. 5 clearly shows that the parameter L is minimum for T_p near to 200 μs and significantly increases when T_p is higher than 500 μs. A shorter value of T_p allows a faster repetition of the decoupling scheme in relation to the $1/J_{CH}$ constant. Furthermore, it has been shown that homonuclear coupling can disturb the decoupling

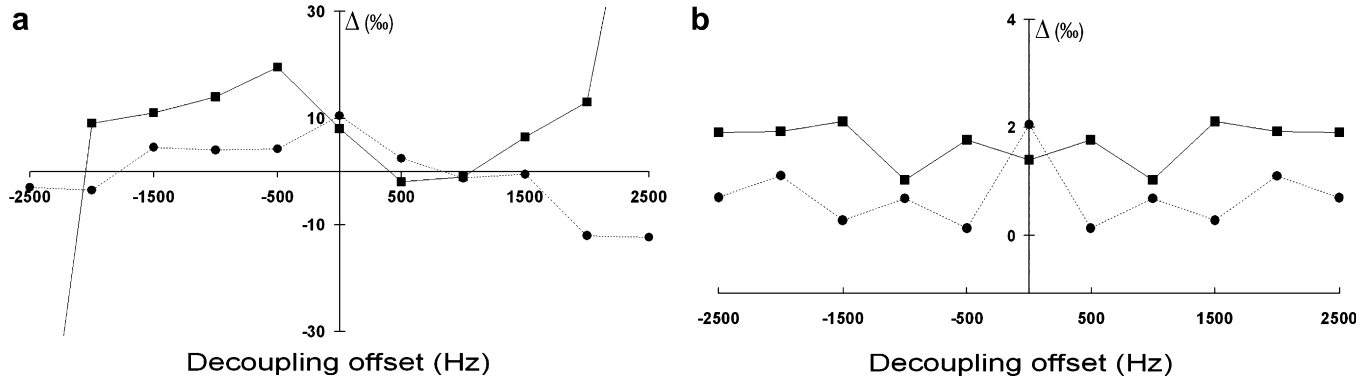

Fig. 6. Δ values (in ‰) as a function of the decoupling offset for the acetic acid molecule (···●···) and for the ethanol molecule -■-). (a) The decoupling was performed using WALTZ-16 with $\omega_2^{\max} = 53.1$ kHz. (b) The decoupling scheme used cos/OIA pulses with $\omega_2^{\max} = 75.2$ kHz, $T_p = 200$ μs, $\Delta F = 14$ kHz and the M4P5–M4P9–M4P5′–M4P9′ cycle. Note the difference in vertical scale between a and b.

efficiency [22] and that there is a direct relationship between this efficiency and the pulse duration [25]. In addition, the K_m calculation does not take into account the influence of instrumental imperfections, such as non-linearity or instability of the decoupler amplifier. The T_p values reported in Fig. 5 were therefore related to all these effects and cannot be explained by taking only the K_m values into account. This is why a comparison with experimental data is essential to avoid erroneous conclusions.

Two hundred microseconds (200 μs) is quite a short duration for an adiabatic pulse and it is not surprising that long phase cycles significantly improve the decoupling performance. Similar results were obtained by Skinner and Bendall [21] with an HS pulse.

After optimization of $\omega_2^{\max}$, ΔF, T_p and the phase cycling, the adiabatic pulse cos/OIA enables an accuracy of 2–3‰ over the decoupled frequency range. The use of acetic acid compared with ethanol highlights that this result is independent of the presence of intramolecular ^{1}H coupling.

Furthermore, although many adiabatic decoupling schemes have already been proposed, the proton decoupling is most often performed with the WALTZ-16 sequence, probably because the aim of these more recent decouplings was essentially to increase the decoupled bandwidth rather than to improve the uniformity of the decoupling. That is why we have compared the performance of the cos/OIA pulse with that of WALTZ-16 in Fig. 6. A dramatic decrease in the parameter L was observed when the cos/OIA was used and the sensitivity to H–H coupling was significantly reduced. The optimized decoupling scheme can therefore be used for proton decoupled quantitative ^{13}C NMR with an expected accuracy near to 2‰.

In this paper, we have examined the performances of four pulse shapes. We have chosen them because they are some of the most studied in previous papers and because of their different properties. The on-resonance adiabaticity of the hyperbolic-secant pulse [14] is independent of the offset Ω [12,13]. However, this is only true when $\omega_2^{\max} = \Delta\omega^{\max}$ [8], which explains why the performance of this pulse was improved by the OIA procedure when $\omega_2^{\max} \neq \Delta\omega^{\max}$ (Fig. 3). The cos/sin pulse [15] enables a time-independent adiabaticity to be obtained for $\Omega = 0$ when $\omega_2^{\max} = \Delta\omega^{\max}$. The on-resonance adiabaticity factor of the WURST-20 pulse [8] is the same for all offsets in the broad central region. The tangential frequency sweep of the tanh/tan pulse [16] allows a linear evolution of the angle θ during the time course of the pulse. Furthermore, thanks to a very slow frequency sweep in the central region and over very wide frequency ranges, high adiabaticity factors can be obtained in the central region.

The $f(\tau)$ function is quite sharp in the case of the HS pulse while it is flatter for WURST-20 or tanh/tan pulses. The cos/sin pulse has an intermediate sharpness. As has previously been shown [12], pulses with the sharpest $f(\tau)$ functions provide the largest K factors but they need a higher peak RF power for the same ω_2^{rms} (Table 1 and [12]). Furthermore, Fig. 3 shows that, when the flatness of the K_m profile is considered, the intermediate shape of the cos/sin pulse gives the best results although the performance of the WURST-20 pulse is not very different.

Clearly, this study does not include all the pulse shapes potentially useful for adiabatic decoupling. However, the strategy proposed can be used to investigate other modulation functions. As an example, the cos^2/OIA pulse (WURST-2) [11], has a value of K_m^{opt} only 3.7% higher than, a peak RF power only 15.5% higher than, and a K_m versus ΔF behavior very close to that of the cos/OIA pulse for the same ω_2^{rms}. It is therefore highly probable that this pulse will give good results.

5. Conclusion

A very flat proton decoupling profile can be obtained thanks to adiabatic pulses while computation of the K_m profile can be used in order to optimize the peak value and the swept frequency range. With cosinus amplitude modulation, offset-independent-adiabaticity, and the M4P5–M4P9–M4P5′–M4P9′ phase cycle, it is possible to reach an accuracy of 2‰ for the ^{13}C NMR measurements.

Our optimization of the adiabatic pulse parameters was based on the minimum adiabaticity. This approach enabled us to achieve our goal in terms of the uniformity of the decoupling. However, further improvements could be obtained by using a more sophisticated approach. For instance, the Numerically Optimized Modulation (NOM) procedure [13], in which the amplitude and frequency modulation functions are simultaneously distorted, ensures that K_m does not fall below a given threshold level for a given range of ω_2^{max} and Ω values.

6. Experimental

6.1. Material

Bi-labeled acetic acid and ethanol in ^{13}C at 99% on the two carbon sites were purchased from Eurisotope, France.

6.2. Sample preparation

Acetic acid: 0.5 ml of the sample was diluted with 0.5 ml of D_2O.

Ethanol: 0.6 ml of the sample was diluted with 0.2 ml of H_2O and 0.2 ml of acetone-d_6.

6.3. NMR experiments

The quantitative ^{13}C NMR spectra were recorded using a Bruker DRX 500 spectrometer fitted with a 5 mm o.d. dual probe $^{13}C/^{1}H$ carefully tuned at the operating frequency of 125.76 MHz. The experiments were performed at 303 K.

The inter-pulse delay (TR) was selected on the basis of the longitudinal relaxation times (ethanol: $T_1^{max} = 16.2$ s and $TR = 114$ s; acetic acid: $T_1^{max} = 27.4$ s and $TR = 192$ s). In order to obtain quantitative measurements for the two sites with an accuracy close to 1‰, a repetition time greater than 7 times the longest T_1, associated with a flip angle of 90° was chosen (pulse width 4.9 μs). The T_1 values were determined by using an inversion recovery sequence, with 12 inversion-time values ranging from 50 ms to 100 s and by using the T_1 processing software of the spectrometer.

The number of points used to define the pulse waveforms was always higher than the product $2.5T_p2\Delta F$ in order to avoid any profile overlapping [26].

Decoupling was applied only during acquisition and a value of 1 s for the sampling period was chosen in order to limit the heating effect of decoupling and to minimize NOE. Furthermore, taking into account the line broadening of 2 Hz, it is sufficient to avoid any truncation of the FID. Measurement conditions were therefore matched to quantitative analysis. A signal-to-noise ratio of 1500 is necessary to achieve an accuracy of 1‰. Consequently, a suitable scan number was chosen according to the respective concentration (NS = 12 for acetic acid and 16 for ethanol).

6.4. Data processing

The free induction decays were processed by an exponential multiplication inducing a line broadening of 2 Hz. The curve fitting was carried out in accordance with a Lorentzian mathematical model using Perch Software (PERCH NMR Software™, University of Kuopio, Finland).

Acknowledgment

The contribution of the Scientific Council of the Region of the Pays-de-la-Loire to the purchase of a 500 MHz spectrometer is gratefully acknowledged.

References

[1] J.K. Lee, A.D. Bain, P.J. Berti, Probing the transition states of four glucoside hydrolyses with ^{13}C kinetic isotope effects measured at natural abundance by NMR spectroscopy, J. Am. Chem. Soc. 126 (2004) 3769–3776, and references therein.
[2] E. Tenailleau, P. Lancelin, R. Robins, S. Akoka, NMR approach to the quantification of non-statistical 13C distribution in natural products: vanillin, Anal. Chem. 76 (2004) 3818–3825.
[3] D.J. Cookson, B.E. Smith, Optimal experimental parameters for quantitative pulse fourier transform proton NMR spectrometry, Anal. Chem. 54 (1982) 2593–2596.
[4] R.R. Ernst, G. Bodenhausen, A. Wokaun, Principles of Nuclear Magnetic Resonances in One and Two Dimensions, Clarendon Press, Oxford, 1987.
[5] E. Tenailleau, G. Remaud, S. Akoka, Quantification of the 1H-decoupling effects on the accuracy of 13C-NMR measurements, Inst. Sci. Tech. 33 (2005) 391–399.
[6] V.J. Basus, P.D. Ellis, H.D.W. Hill, J.S. Waugh, Utilization of chirp frequency modulation with 180-phase modulation for heteronuclear spin decoupling, J. Magn. Reson. 35 (1979) 19–37.
[7] Z. Starcuk, K. Bartusek, Z. Starcuk, Heteronuclear broadband spin-flip decoupling with adiabatic pulses, J. Magn. Reson. A 107 (1994) 24–31.
[8] E. Kupce, R. Freeman, Stretched adiabatic pulses for broadband spin inversion, J. Magn. Reson. A 117 (1995) 246–256.
[9] E. Kupce, R. Freeman, Adiabatic pulses for wideband inversion and broadband decoupling, J. Magn. Reson. A 115 (1995) 273–276.
[10] E. Kupce, R. Freeman, Decoupling: theory and practice I, NMR Biomed. 10 (1997) 372–380.
[11] E. Kupce, R. Freeman, Optimized adiabatic pulses for wideband spin inversion, J. Magn. Reson. A 118 (1996) 299–303.
[12] A. Tannus, M. Garwood, Improved performance of frequency-swept pulses using offset-independent adiabaticity, J. Magn. Reson. A 120 (1996) 133–137.
[13] M. Garwood, L. DelaBarre, The return of the frequency sweep: designing adiabatic pulses for contemporary NMR, J. Magn. Reson. 153 (2001) 155–177.
[14] M.S. Silver, R.I. Joseph, D.I. Hoult, Highly selective p/2 and p pulse generation, J. Magn. Reson. 59 (1984) 347–350.
[15] M.R. Bendall, D.T. Pegg, Uniform Sample Excitation with Surface Coil for In Vivo Spectroscopy by Adiabatic Rapid Half Passage, J. Magn. Reson. 67 (1986) 376–381.
[16] C.J. Hardy, W.A. Edelstein, D. Vatis, Efficient adiabatic fast passage for NMR population inversion in the presence of radiofrequency field inhomogeneity and frequency offsets, J. Magn. Reson. 66 (1986) 470–482.
[17] M.R. Bendall, T.E. Skinner, Calibration of STUD+ parameters to achieve optimally efficient broadband adiabatic decoupling in a single transcient, J. Magn. Reson. 134 (1998) 331–349.

[18] E. Kupce, R. Freeman, An adaptable NMR broadband decoupling scheme, Chem. Phys. Lett. 250 (1996) 523–527.
[19] E. Kupce, R. Freeman, G. Wider, K. Wüthrich, Suppression of cycling sidebands using bi-level adiabatic decoupling, J. Magn. Reson. A 122 (1996) 81–84.
[20] T.E. Skinner, M.R. Bendall, A vector model of adiabatic decoupling, J. Magn. Reson. 134 (1998) 315–330.
[21] T.E. Skinner, M.R. Bendall, A phase-cycling algorithm for reducing sidebands in adiabatic decoupling, J. Magn. Reson. 124 (1997) 474–478.
[22] A.J. Shaka, C.J. Lee, A. Pines, Iterative schemes for bilinear operators; application to spin decoupling, J. Magn. Reson. 77 (1988) 274–293.
[23] M.H. Levitt, R. Freeman, Composite Pulse Decoupling, J. Magn. Reson. 43 (1981) 502R–507R.
[24] Tycko, A. Pines, J. Guckenheimer, Fixed point theory of iterative excitation schemes in NMR, J. Chem. Phys. 83 (1985) 2775–2802.
[25] T. Fujiwara, K. Nagayama, Efficiency of heteronuclear broadband decoupling and homonuclear cross-polarization analyzed on two time scales, J. Magn. Reson. 81 (1989) 245–254.
[26] M.R. Bendall, T.E. Skinner, Calibration of STUD decoupling to Achieve Selected Sideband Amplitudes, J. Magn. Reson. A 120 (1996) 77–87.